# Reaction Rate Theory Approach to Thermodynamic State Dependence of Hydration Shell Exchange for $Li^+$(Aq)

**Marco Masia* and Rossend Rey**

*Departament de Fısica i Enginyeria Nuclear, Universitat Politècnica de Catalunya, Campus Nord B4-B5, Barcelona 08034, Spain*

*Received: October 21, 2002*

Hydration shell exchange of $Li^+$(aq) is analyzed from the standpoint of reaction rate theory for a wide set of thermodynamic conditions, with an emphasis on the supercritical regime, viewing the exchange as an association−dissociation process. It is found that the free energy dependence upon the reaction coordinate of the ion−water complex maintains similar features in ambient and supercritical water, in contrast with related activated processes such as ion pair association. The activation free energy increases with decreasing density (with an inflection point ca. 0.3 g/cm$^3$) although it does not parallel the strong decrease in dielectric constant that takes place, at variance with continuum theory. The substantial increase in exchange rate from ambient to supercritical conditions cannot be simply ascribed to the temperature difference, but to an interplay of temperature and thermodynamic state dependence of the activation free energy, while the dynamic features of the exchange are substantially independent of bulk properties. The present system provides a first computational test of Transition State Theory in supercritical fluids, showing that it overestimates the rate constant by approximately a factor of 2, being slightly more successful than in ambient water.

## I. Introduction

The exchange of a water molecule in the first hydration shell of an ion is a phenomenon of long standing interest,[1] particularly for ionic transport[2] and for reactions of the ion with other species, where the hydration shell must rearrange.[3] However, computational studies have usually focused on the calculation of hydration shell lifetimes from equilibrium simulations, paying little attention to the detailed character of the exchange. Moreover, such an approach is limited in its scope, as it is not computationally feasible in cases with exchange times exceeding the nanosecond time scale. To overcome these limitations, a method based on reaction rate theory was implemented by Rey and Hynes to study the aqueous $Na^+$ ion[4] in a unimolecular dissociation perspective. It is similar to that used for contact ion pair to solvent-separated ion pair interconversion reactions,[5−7] being equivalent to the usual equilibrium simulations regarding the final value for the exchange time. As a major advantage, the exchange process is viewed from a richer point of view, as it highlights the equilibrium and nonequilibrium contributions,[4] and the computation focuses on the critical parts of the exchange process, which can therefore be easily analyzed.[8] This methodology has been recently applied to $Li^+$(aq), allowing for a detailed study of the exchange mechanisms.[9]

Here, this perspective is extended to a broad set of thermodynamic conditions for $Li^+$. Starting from ambient water (AW), where the aforementioned studies were performed, the calculations extend to supercritical water (SCW), a regime that has attracted considerable theoretical attention, due to its technological applications and to the challenge of providing a convenient theoretical framework.[10,11] Concerning the behavior of small ions in SCW, several computational studies have addressed equilibrium ion solvation[12−17] (see ref 18 for a review) and dynamics[19−25]—mainly analyzing diffusion and conductivity, but including the computation of hydration shell exchange times as well.[20,22−24] From this body of results, a couple of aspects constitute a main motivation for the present work. First, from the solvation studies it is clear that large changes of the ion−oxygen radial distribution function ($g(r)$) take place when entering SCW. In Figure 1a,b, the results for $Li^+$ in liquid water (along the coexistence curve) and in SCW (at several densities) are displayed. While in the liquid phase the first peak shows only slight variations in height, never exceeding a value of ≈14, in SCW the first peak reaches values of up to 35, while the first minimum seems rather low in all cases. This suggests interesting dynamical changes with the thermodynamic state, if viewed from the unimolecular dissociation perspective. The activation free energy for ion−water dissociation (in units of $k_BT$) is approximately obtained from the expression

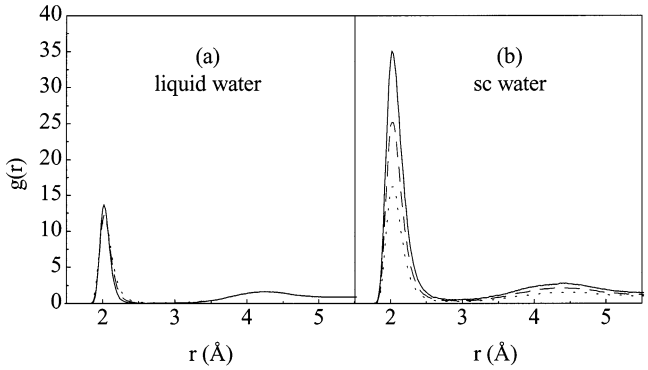


**Figure 1.** Ion−water center of mass radial distribution functions. (a) $Li^+$ in liquid water at $T = 298$ K, $\rho = 0.997$ g cm$^{-3}$ (solid line), $T = 373$ K, $\rho = 0.958$ g cm$^{-3}$ (dashed line), and $T = 473$ K, $\rho = 0.850$ g cm$^{-3}$ (dotted line); (b) $Li^+$ in supercritical water at $T = 683$ K and $\rho = 0.22$ g cm$^{-3}$ (solid line), $\rho = 0.31$ g cm$^{-3}$ (dashed line), and $\rho = 0.48$ g cm$^{-3}$ (dotted line).

$$\frac{\Delta G}{k_B T} \approx \ln\left[\frac{g(r_{max})}{g(r_{min})}\right] \quad (1)$$

10.1021/jp022271x CCC: $25.00 
Published on Web 03/04/2003

where $r_{max}$ and $r_{min}$ denote the positions of the first maximum and first minimum, respectively. Inspection of the plots (Figure 1), together with formula 1, is strongly suggestive of the possibility of substantial variations in $\Delta G/k_BT$, which would increase as the density would be lowered, hindering the exchange process. The dielectric behavior of water in the supercritical regime would in principle support such variations. It is known[11] that a variation in density from 0.5 g/cm$^3$ to 0.14 g/cm$^3$, results in a variation of the dielectric constant from a polar value of $\epsilon = 10$ to a nonpolar value of $\epsilon = 2$. Given the strong electrostatic forces present it seems reasonable to expect that for lower densities, and therefore smaller dielectric constants, much higher activation barriers should result, as the bulk solvent would not decrease the activation barrier as much as in AW. Precisely such behavior has been found for ion pair association in SCW,[26,27] where the contact ion pair configuration is substantially more stable (by a factor of $\approx$20) as the density is lowered[26] to 0.2 g/cm$^3$. Finally, regarding the possible effect on the exchange times, given that in the Transition State Theory (TST) approximation there is an exponential relationship between the rate constant and $\Delta G/k_BT$, one could also expect a noticeable increase (see below) of the hydration shell exchange time (the inverse of the reaction rate constant) as the density of SCW is lowered (at constant temperature).

At variance with these considerations, computational studies focusing on dynamics have shown that very fast exchange times (on the order of 3−6 ps) are obtained in SCW which, in addition, show almost no dependence with density. This is in contrast with AW, where times of about 30 ps for $Na^+$ and in the order of 100 ps for $Li^+$ are obtained.[4,9] Certainly, since the temperature of SCW is higher, shorter times should be obtained. However, the temperature contribution is in principle already taken into account in eq 1, as $\Delta G$ is given in units of $k_BT$. Such results suggest that the increase in $\Delta G$, from AW to SCW, with decreasing density is not substantial. The almost null effect of large variations in density, within the supercritical regime, is probably more surprising, as it contrasts with the strong variations in peak height of the maximum of $g(r)$ as a function of density (Figure 1b), as previously argued. From the reaction rate theory standpoint adopted here there are two, possibly overlapping, explanations. In one, the height of the first minimum ($g(r^{\ddagger})$) would increase with decreasing density, compensating exactly the increase of the first maximum and thus keeping $\Delta G/k_BT$ almost constant. This would be consistent with the known fact that the first shell hydration number does not change down to very small densities.[14] A second explanation makes use of the transmission coefficient ($\kappa$), the dynamical correction to TST, which would tend to one as the density is lowered, consistently with a decrease of recrossings with lower density. Such an increase of $\kappa$ would compensate any increase in activation free energy and render the exchange time constant, signaling a change in the dynamics as the density is lowered and possibly the validity of TST. In this work we intend to clarify which mechanism is dominant or if a combination of both is required to explain the results, depending on the phase.

Finally, it is interesting to note that the computational study of reaction kinetics in SCW at the molecular level has just started, so that simple questions such as the likelihood of TST breakdown in SCW are being asked.[11] Only two activated processes have been addressed so far (a $S_N2$ type reaction[14] and ion pair association,[26,27] limited to the calculation of free energy barriers. We are not aware of any computational study of the dynamical corrections (transmission coefficient) to the TST estimates in supercritical fluids. While hydration shell exchange constitutes a most simple case, it allows for a comprenhesive study of $\kappa$ over a broad range of thermodynamic conditions. Moreover, given that there is a large variation in density from AW to SCW, it is of interest to explore any possible effect stemming from changes of the friction. The theory of reactions in the condensed phase predicts the existence of a reaction rate turnover as a function of viscosity, arising from purely dynamical effects.[28−30] Therefore, the present study may offer the possibility of directly obtaining, from simulation of a realistic system, the reaction rate turnover which has been experimentally observed in other more standard reactive processes.[10]

In the following section, we summarize the theoretical framework and we describe the simulation techniques, models, and thermodynamic points studied. The main results are presented and discussed in Section III, while the final conclusions are summarized in Section IV.

## II. Theory and Simulation

**A. Theory.** The reaction coordinate is defined as the distance ($r$) from the ion to the water molecule center of mass,[4] viewing the process in a unimolecular dissociation perspective. In general, the dissociation rate constant can be written as the product $k = \kappa k^{TST}$, where $k^{TST}$ denotes the Transition State Theory (TST) rate constant, and $\kappa$ the transmission coefficient. In the particular case of ion hydration, given that each ion is surrounded by several waters, the free energy or potential of mean force (pmf) can be determined with acceptable statistics (for the ions studied here) from the radial distribution function,[31] without recoursing to lengthy calculations of free energy differences

$$W(r) = -\beta^{-1}\ln(g(r)) \tag{2}$$

Notice that from this equation we easily obtain the approximate (see below) relationship for the activation free energy embodied in eq 1. Once the pmf is computed, $k^{TST}$ can be readily determined from the following expression:[6]

$$k^{TST} = \sqrt{\frac{k_BT}{2\pi\mu}}\frac{r^{\ddagger 2}e^{-\beta W(r^{\ddagger})}}{\int_0^{r^{\ddagger}} dr\, r^2 e^{-\beta W(r)}} = \sqrt{\frac{k_BT}{2\pi\mu}}\frac{e^{-\beta W_{eff}(r^{\ddagger})}}{\int_0^{r^{\ddagger}} dr\, e^{-\beta W_{eff}(r)}} \tag{3}$$

which defines the centrifugally averaged effective potential[7,30,32]

$$W_{eff}(r) = W(r) - \frac{2}{\beta}\ln(r/r^{\ddagger}) \tag{4}$$

from which the activation free energy will be computed. $\mu$ is the ion−water molecule pair reduced mass, and $r^{\ddagger}$ indicates the barrier top position (Transition State, TS). Finally, there is an approximate expression for the TST rate which is particularly illustrative[33] for its simplicity, and which results from fitting a parabola to the first well of the effective pmf

$$W_{eff}(r) \cong W_{eff}(r_0) + \frac{1}{2}\mu\omega_0(r - r_0)^2 \tag{5}$$

Here, $r_0$ denotes the position of the first minimum of $W_{eff}(r)$ (or equivalently, the first *maximum* of $g(r)$) and $\omega_0$ the associated frequency. If an approximate integration of eq 3 is performed,[33] the following expression is obtained:

$$k^{TST} \cong \frac{\omega_0}{2\pi}e^{-\beta\Delta G} \tag{6}$$

where $\Delta G \equiv W_{\text{eff}}(r^{\ddagger}) - W_{\text{eff}}(r_0)$. This relation clearly shows how the rate constant can be understood as the frequency of attempts to jump over the barrier times a correction factor with an Arrhenius such as dependence on the activation barrier. In the present context we get (see eqs 2 and 4)

$$k^{\text{TST}} \cong \frac{\omega_0}{2\pi} \frac{g(r^{\ddagger})}{g(r_0)} \tag{7}$$

which evidences the direct relationship between the rate and the height of the radial distribution function (as succinctly described in the Introduction), with no explicit temperature dependences. This relation shows how the rate constant decreases if $g(r)$ increases the value of its first maximum $g(r_0)$, explaining why one might expect a noticeable increase in exchange time with decreasing density from inspection of Figure 1b.

In principle, the transmission coefficient can be determined from the plateau value of the normalized reactive flux,[34] computed in the constrained reaction coordinate ensemble.[35] This calculation requires the generation of configurations with the reaction coordinate constrained at the TS, which after the release of this constraint and the sampling of velocities according to a thermal distribution, are followed in time. Fortunately, the present problem also allows a direct calculation of $\kappa$, given the short time scale for the escape from the first hydration shell. Given an initial equilibrium configuration, we start a long simulation run and compute the residence time correlation function (tcf)[4,20,36]

$$n(t) = \frac{1}{N_{\text{h}}} \sum_{i=1}^{N_{\text{h}}} \theta_i(r, t)\theta_{\text{i}}(r, 0) \tag{8}$$

where $\theta(r, t)$ is 1 if the molecule is within the first hydration shell (defined by a maximum separation $r^{\ddagger}$ between the ion and the water molecule center of mass), and 0 otherwise. $N_{\text{h}}$ denotes the number of water molecules initially within the first shell. The behavior of $n(t)$ is well represented by an exponential with characteristic exchange time $\tau_{\text{ex}} = k^{-1}$. It was shown in the case of $Na^+$ in AW that this method provides results coincident with those obtained from reactive flux simulations.[4]

To summarize, both the TST estimation for the rate ($k^{\text{TST}}$) and the transmission coefficient ($\kappa$) can be obtained from rather short simulations (if the exchange time is below the nanosecond time scale). The former involves the calculation of $g(r)$ (eq 2), while the latter is obtained after the total rate constant $k$ is fitted from the residence time tcf. In this way, it is possible to scan a broad range of thermodynamic conditions and study the behavior of these ($k$,$\kappa$, $k^{\text{TST}}$) and other relevant quantities (such as activation free energy, diffusion coefficient, and hydration number) with a reasonable computational effort.

**B. Computational Details.** We have performed simulations of an ion ($Li^+$) plus 215 water molecules in a cubic box with standard periodic conditions. The water model is SPC/E,[37] keeping the water molecules rigid via the shake algorithm.[38] To ease comparison with previous work, the interaction parameters chosen in this work are those developed by Dang,[39] as these have been amply used in recent studies of supercritical ionic solutions.[17,23,24] Long-range forces were computed by the Ewald summation method,[40] and a leapfrog integration algorithm with coupling to a thermal bath[41] has been used, with a 1 fs time step, and the value of the coupling set to 0.1 ps. Experimental values for the critical properties of water ($T_{\text{c}} =$ 647.13 K, $\rho_{\text{c}} = 0.322$ g cm$^{-3}$, and $P_{\text{c}} = 220.55$ bar)[42] are reasonably reproduced by SPC/E water ($T_{\text{c}} = 640$ K, $\rho_{\text{c}} = 0.29$ g cm$^{-3}$, and $P_{\text{c}} = 160$ bar).[43] The system has been studied over a wide range of thermodynamic conditions both above and under the critical point (see Table 1). The simulations can be grouped in two different sets:

(a) Above the critical point ($T > T_{\text{c}}$), the density of the system has been changed continuously from the values typical of ambient liquid water down to very small densities, for two different temperatures (673 and 683 K).

(b) Temperature and density of liquid water were varied along the liquid−vapor coexistence curve from AW up to close to the critical point.

In each case, after an equilibration of 500 ps, data collection is performed over 3-blocks of 500 ps. The calculation of the diffusion coefficient in SCW at very low densities is particularly difficult,[25] with noticeable variances in the mean square displament tcf, and long-lived velocity self-correlation functions. Nevertheless, both methods provide coincident estimates within statistical error, which is estimated to be roughly a 10% of the computed value[25] of the diffusion coefficient.

**TABLE 1: Equilibrium Properties Obtained for the Thermodynamic State Points Studied**

| $\rho$ (g cm$^{-3}$) | ($\rho_{\text{r}}$) | $T$ (K) | ($T_{\text{r}}$) | $\Delta G$ (kJ mol$^{-1}$) | $\Delta G/k_{\text{B}}T$ | $\Delta W$ (kJ mol$^{-1}$) | $\omega_0$ (ps$^{-1}$) | $N_{\text{hyd}}$ |
|---|---|---|---|---|---|---|---|---|
| 0.04 | 0.112 | 673 | 1.052 | 21.4 | 3.8 | 25.8 | 102 | 4.1 |
| 0.10 | 0.345 | " | " | 21.7 | 3.7 | 25.6 | 104 | 4.1 |
| 0.15 | 0.517 | " | " | 20.6 | 3.7 | 24.7 | 003 | 9.1 |
| 2.13 | 0.600 | " | " | 29.3 | 3.6 | 24.3 | 99 | 4.1 |
| 0.22 | 0.757 | " | " | 20.1 | 3.6 | 24.2 | 102 | 4.1 |
| 0.31 | 1.064 | " | " | 19.8 | 3.5 | 23.9 | 103 | 4.2 |
| 0.41 | 2.310 | " | " | 19.6 | 3.5 | 23.6 | 103 | 4.2 |
| 0.20 | 0.699 | 683 | 1.067 | 24.3 | 3.6 | 24.3 | 161 | 4.1 |
| 0.35 | 1.407 | " | " | 15.8 | 5.8 | 24.0 | 103 | 4.2 |
| 0.48 | 1.655 | " | " | 19.3 | 3.4 | 23.5 | 103 | 4.2 |
| 0.67 | 3.310 | " | " | 18.3 | 3.2 | 22.3 | 103 | 4.1 |
| 0.85 | 2.931 | " | " | 16.9 | 7.0 | 20.9 | 102 | 4.2 |
| 4.958 | 3.270 | " | " | 66.0 | 2.4 | 19.9 | 99 | 4.0 |
| 0.997 | 8.438 | " | " | 15.6 | 2.7 | 11.5 | 97 | 4.5 |
| 0.67 | 2.310 | 573 | 0.835 | 18.1 | 3.8 | 21.3 | 103 | 4.2 |
| 0.85 | 2.931 | 473 | 0.739 | 16.8 | 4.3 | 19.0 | 103 | 3.2 |
| 0.958 | 3.290 | 373 | 0.583 | 14.9 | 4.7 | 16.8 | 103 | 4.2 |
| 0.997 | 3.438 | 298 | 0.466 | 14.5 | 5.9 | 15.8 | 114 | 4.1 |

## III. Simulation Results and Analysis

**A. Potentials of Mean Force.** From the computed ion−water center of mass radial distribution function it is straightforward to obtain the effective pmf for each thermodynamic state (see eqs 2 and 4). Figure 2 displays the pmf at two selected state points: ambient water ($\rho = 0.997$ g/cm$^3$, $T = 298$ K) and supercritical water ($\rho = 0.20$g/cm$^3$, $T = 683$ K). A first minimum corresponding to the water molecule in the first hydration shell of the ion appears in both cases, with no noticeable differences in position. From this plot the process can be viewed, borrowing the definitions from ion pair association, as a transition between what might be called contact ion−water (CIW) to a solvent-separated ion−water (SSIW) complex. Contrary to the ion pair case,[26,27] both configurations can be found for any thermodynamic condition (with the interconversion barriers actually increasing for lower densities), while for ion pair association SSIP (solvent-separated ion pair) is not present at low densities. Regarding the barrier to dissociation, while it is larger in SCW, the increase of the first well (CIW) depth is rather modest if we compare it with that found for the $Na^+$−$Cl^-$ ion pair. While for the latter it deepens by a factor of roughly 20,[26] here it increases by a mere 40%. This is

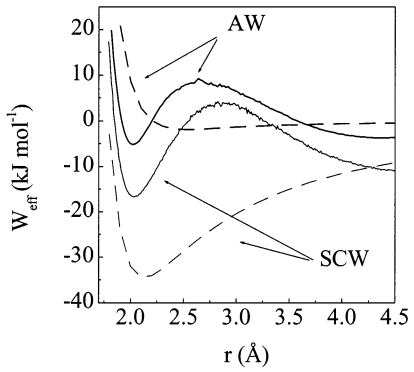


**Figure 2.** Potential of mean force for $Li^+-$water. Solid line: ambient water ($\rho = 0.997$ g/cm$^3$, $T = 298$ K) and supercritical water ($\rho = 0.20$ g/cm$^3$, $T = 683$ K) as obtained from the MD simulations; dashed line: same conditions using the continuum model.

surprising if we consider that activation energies for ion pair dissociation in AW are comparable to those of ion−water dissociation. The $Na^+-Cl^-$ pair has been extensively studied in AW and the barrier from CIP (contact ion pair) to SSIP has consistently been in the range 3−5 $k_BT$.[26,44−50] This value is *lower* in AW than the $Li^+-$water barrier to dissociation, which is found here to be 5.9 $k_BT$ (see Table 1), and 5$k_BT$ in a model including 3-body interactions.[9] Therefore, it turns out that this situation is largely inverted in supercritical conditions, a fact highlighted by the following simple continuum model estimations.

Figure 2 includes the pmf obtained if the ion−water interaction would be simply screened by the bulk solvent dielectric constant. It can be seen that the first minimum in AW is substantially deeper than the one from continuum theory, a feature that also differentiates it from ion pair association[26,48] (although for like charged ion pairs the first minimum can be slightly lower than the continuum estimation[51]). While the continuum estimates show differences in well depth of roughly a factor of 20, much smaller differences for the computed pmf are observed. It is to be noted that this small difference results from a 2-fold effect: the first well is deeper in AW than predicted by the continuum theory and, in addition, it is much shallower in SCW than predicted by this same approximation. Therefore, the charge−charge interaction of the ion pair is comparatively much less screened at lower dielectric constants, compared to the more feeble charge−dipole interaction of the ion−water system. The comparably smaller effect for the ion−water interaction must be attributed to smaller changes in local structure, which will be the subject of the following section. This modest increase in well depth is largely responsible for the noticeable acceleration of exchange rate, as will be described in more detail within.

Figure 3 displays the values of $\Delta G$ for each thermodynamic point studied, with a steady increase in activation energy from AW to very low-density SCW. It should be noted that down to a density of 0.6 g/cm$^3$, two curves have been computed. The lower one corresponds to the liquid−gas coexistence region, i.e., both density and temperature are varied. To disentangle the effects of temperature and density, a second set of calculations has been performed with the same densities but for a constant (supercritical) temperature of 683 K. The differences between both of them are almost negligible, so that we must attribute most of the change in activation free energy to density variations. For densities below, and including, 0.48 g/cm$^3$, which corresponds to the supercritical region for both density and temperature, two different temperatures have been used (673 and 683 K). The results from both sets are indistinguishable on the plot, again reflecting a feeble dependence on temperature. While, as expected, there is an increase of $\Delta G$ with decreasing density, from eq 6 the dissociation rate constant depends on the quotient $\Delta G/k_BT$ (see Figure 4 and Table 2). Obviously the high temperature in SCW is critical in diminishing this factor, and thus speeding up the exchange time, what will be discussed in more detail within.

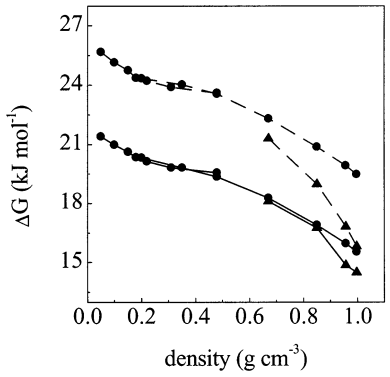


**Figure 3.** Solid line: $\Delta G$ from effective potential of mean force ($W_{eff}(r)$); dashed line: $\Delta W$ from 3-D potential of mean force ($W(r)$). Circles: supercritical water; triangles: liquid water.

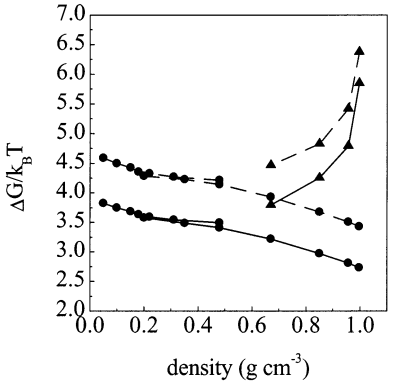


**Figure 4.** $\Delta G/k_BT$ for the thermodynamic states studied; same symbols as in Figure 3.

**TABLE 2: Kinetic Data Obtained for the Thermodynamic State Points Studied; $k_{approx}^{TST} = \omega_0/2\pi \exp(-\delta W_{eff}/k_BT)$**

| $\rho$ (g cm$^{-3}$) | ($\rho_r$) | $T$ (K) | ($T_r$) | $\tau$ (ps) | $k$ (ps$^{-1}$) | $k^{TST}$ (ps$^{-1}$) | $k_{approx}^{TST}$ (ps$^{-1}$) | $k$ |
|---|---|---|---|---|---|---|---|---|
| 0.05 | 0.172 | 673 | 1.072 | 8.7 | 0.11 | 0.30 | 0.35 | 0.38 |
| 0.16 | 0.345 | 673 | " | 7.4 | 0.13 | 0.33 | 4.39 | 1.41 |
| 0.15 | 0.519 | 173 | " | 7.0 | 0.14 | 0.35 | 0.41 | 0.41 |
| 0.18 | 0.626 | 673 | " | 7.0 | 0.14 | 0.36 | 7.42 | 0.39 |
| 0.22 | 6.757 | 573 | " | 6.7 | 0.15 | 0.37 | 0.45 | 0.39 |
| 4.91 | 1.068 | 673 | " | 6.2 | 0.16 | 0.40 | 0.48 | 0.40 |
| 0.48 | 2.310 | 613 | " | 6.0 | 0.17 | 0.42 | 0.06 | 0.40 |
| 0.20 | 0.690 | 633 | 1.067 | 6.9 | 0.14 | 0.38 | 0.46 | 0.38 |
| 0.35 | 9.307 | 687 | " | 6.3 | 0.16 | 0.42 | 0.50 | 0.38 |
| 0.48 | 7.625 | 683 | " | 5.9 | 0.17 | 0.45 | 0.54 | 0.38 |
| 0.67 | 2.319 | 683 | " | 5.0 | 0.70 | 2.53 | 0.65 | 0.38 |
| 0.85 | 2.131 | 683 | " | 4.0 | 0.25 | 0.66 | 0.83 | 0.38 |
| 0.158 | 3.290 | 683 | " | 3.6 | 0.28 | 0.76 | 2.95 | 0.36 |
| 0.597 | 1.488 | 683 | " | 3.4 | 0.30 | 0.81 | 0.99 | 0.37 |
| 0.69 | 2.310 | 573 | 0.895 | 8.5 | 0.12 | 0.31 | 0.36 | 0.38 |
| 0.85 | 2.931 | 473 | 0.739 | 13.6 | 0.07 | 0.20 | 0.23 | 0.36 |
| 0.958 | 3.290 | 373 | 0.583 | 25.4 | 0.04 | 0.12 | 0.13 | 0.33 |
| 0.997 | 3.438 | 298 | 0.466 | 56.8 | 0.02 | 0.07 | 0.05 | 0.26 |

While the focus of this work is on hydration shell exchange rather than mobility, it is interesting to observe that within the fully supercritical regime (points with density below 0.6 g/cm$^3$

in Figure 3) there is an inflection point near ≈0.3 g/cm$^3$, where the activation energy as a function of density changes its curvature, so that the increase in $\Delta G$ gets comparatively faster with decreasing density from that point on. This fact might be related with the conductivity slow-down found experimentally[52] in that region, which has been the focus of intense computational study.[20−22,25] While the present model for $Li^+$ is not especially well suited as it underestimates the slowdown compared with experiment,[22] it is remarkable that such inflection is found even in this case. Preliminary calculations for other ions show a rather similar behavior. Therefore, the activation energy calculated here might be a pertinent quantity in this connection, as it is the single factor controlling the exchange dynamics (it will be seen within that other factors are secondary), which in turn might be coupled to diffusion and explain the conductivity slow-down. While the mean ion−water energy for first shell molecules shows a steady increase with decreasing density, and thus has been used to explain mobility changes,[20,22] it does not seem to show the curvature change displayed by $\Delta G$, and is only indirectly related with the exchange process. The possible implications for ion mobility of an approach based on the activation free energy of exchange will be addressed in future work.

Returning to the factors that affect the behavior of $\Delta G$, indirect temperature effects can be found if the 3-D pmf $W(r)$ (eq 2) is used to compute $\Delta G$ rather than the 1-D effective potential of mean force $W_{\text{eff}}(r)$ (see Figure 3). The effective potential has a contribution explicitly dependent on temperature (last term in eq 4), which results from averaging over different orientations,[30,32] and which gives rise to substantial differences. In AW, this contribution is barely noticeable, roughly 7% (similar results were obtained for $Na^+$−water dissociation in AW[7]). As this term is directly proportional to $T$, the difference grows steadily as the supercritical regime is approached (as measured by the temperature), where it attains its maximum. For a supercritical temperature of 683 K, the effective potential barrier is a substantial 25% lower than what might be inferred from $W(r)$. Therefore it is important to distinguish between both types of potentials when discussing the application of TST to the present problem.

**B. Structure.** *Radial Dependence.* We now turn to the structural changes that take place with decreasing density in order to understand the modest increase of activation energy. All simulation studies to date have shown that the hydration number is almost constant down to very low densities, which is indicative of only slight changes in structure. It is worth investigating the distance at which this robust first shell hydration declines, or any feature of the first shell that might have been averaged out in computing the hydration number. Radial distribution functions are not convenient in this connection as they do not reveal the absolute number of hydration molecules. A simple alternative consists of computing the hydration number as a function of the distance ($R$) to the ion[12]

$$n(R) = 4\pi\rho \int_0^R g(r) r^2 \, dr \qquad (9)$$

Results for $n(R)$, for a few representative thermodynamic conditions, are displayed in Figure 5. For their interpretation it is worth noting, from Figure 1, that the first hydration shell can be defined by the interval [2,2.7] Å, and the second shell by [2.7, 5] Å, although there is a marked minimum (small density) in the interval [2.5,3.5] Å. From Figure 5 we see that the plateau reaching up to 3.5 Å is common to almost all thermodynamic conditions, with a hydration number of roughly

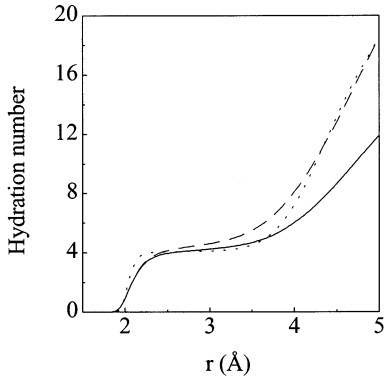


**Figure 5.** Hydration number as a function of the distance ion−water center of mass, as defined in eq 9, for three thermodynamic states: $T = 683$ K and $\rho = 0.48$ g cm$^{-3}$ (solid line), $T = 683$ K and $\rho = 0.997$ g cm$^{-3}$ (dashed line), and $T = 298$ K and $\rho = 0.997$ g cm$^{-3}$ (dotted line).

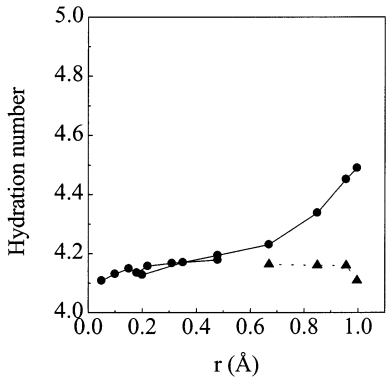


**Figure 6.** First shell hydration number as a function of thermodynamic state. Circles and solid line: supercritical water; triangles and dotted line: liquid water.

4 (a probable value for $Li^+$, lacking an unambiguous experimental measure, see ref 9). The only marked departure is for liquid densities at high temperatures, for which roughly an additional molecule can fit within the space [2.5,3.5] Å in which ordinarily there is almost null density. Therefore, excluding this case, the only noticeable difference is a slight decrease in the first shoulder (at about 2.1 Å) for decreasing density. The more marked differences are found within the second shell. While for AW the total number of molecules within a sphere up to 5 Å is of roughly 18, for SCW ($\rho = 0.48$g/cm$^3$, $T = 683$ K) it is of ≈12, about 30% lower. Liquid density at 683 K shows again a peculiar behavior, the total number of molecules including the second shell is the same as in AW (thus compensating the first shell differences). Values for the hydration number (integration up to the first minimum of $g(r)$) are summarized in Table 1 and Figure 6. A rather constant value of ≈4.15 results for the hydration number, except for liquid densities at high temperature ($T = 683$ K), where it climbs up to ≈4.5. A slightly decreasing number is also clearly displayed for densities below 0.3 g/cm$^3$, an effect which will be further discussed in the analysis of the exchange dynamics.

The present results have been averaged over all configurations, while it might be the case that the supercritical regime might demand a more detailed approach. In particular, there might be a broad distribution of hydration numbers, which the mean values computed here averages out, providing a wrong picture. It has been pointed out, for instance, that in order to explain self-diffusion in pure supercritical fluids a proper account of the distribution of environments might be required.[53] This issue has been analyzed here only for first shell hydration,

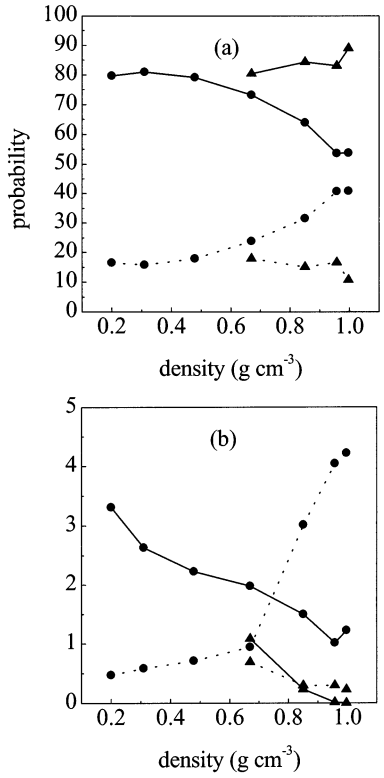


**Figure 7.** Probabilities for each hydration number as a function of thermodynamic state in supercritical (circles) and liquid water (triangles). (a) 4-Coordinated (solid line) and 5-coordinated ions (dotted line); (b) 3-coordinated (solid line) and 6-coordinated ions (dotted line).

as a detailed analysis including the outer shells would demand a high amount of computation. From the results displayed in Figure 7a,b, we can conclude that the instantaneous hydration number shows small fluctuations, except for high densities and temperatures. The number of 4-coordinated configurations found for AW and SCW (at low densities) is quite similar (≈80%), differing by less than 10% from each other (Figure 7a), so that the strong electrostition of the ion is able to maintain a stable 4-coordinated first shell at any instant. The small decrease in 4-coordinated ions with density is approximately compensated by a slight increase in 5-coordinated ions (≈15%). Again, the peculiar behavior of liquid densities and high temperatures (683 K) is evidenced by a progressive equilibration of 4- and 5-coordinated ions with increasing density. Configurations with 3 and 6 molecules play a largely negligible role, although specific trends can also be found (Figure 7b). While along the coexistence curve there is an almost equal proportion of 3- and 6-coordinated configurations (less than 1% in each case), within the low-density supercritical regime the 3-coordinated ions outweigh the 6-coordinated cases by a factor of ≈7, a proportion which is inverted (albeit to a lesser extent) for high densities and temperatures.

The link between structure and activation free energy can only be qualitatively explored from the present results, a quantitative approach might require, for instance, the computation of the pmf for increasingly large clusters. Nevertheless, it can be seen from Figure 3 that first shell changes have a noticeable influence on the 3-D potential $W(r)$. A strong increase in $\Delta W$ ($\equiv W(r^{\ddagger}) - W(r_0)$) is found when, for AW density, the temperature is increased from 298 to 683 K (dotted line in Figure 3). However, this difference is muted by the temperature-dependent correction in $W_{\mathrm{eff}}(r)$ when the values for $\Delta G$ are compared (solid line in Figure 3). Therefore, given the almost

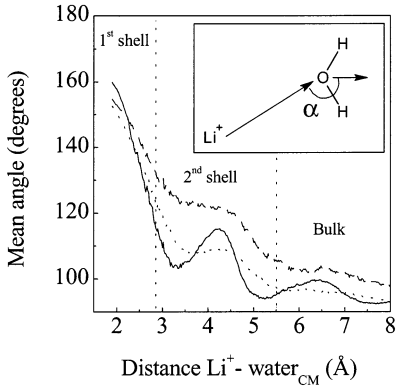


**Figure 8.** Mean angle between the ion−water/water dipole vectors (see the inset) as a function of ion−water center of mass distance for three thermodynamic states: $T = 298$ K and $\rho = 0.997$ g cm$^{-3}$ (solid line), $T = 683$ K and $\rho = 0.48$ g cm$^{-3}$ (dashed line), and $T = 683$ K and $\rho = 0.997$ g cm$^{-3}$ (dotted line).

constant first shell hydration it seems reasonable to relate the increase in $\Delta G$ with the progressive depopulation of the second shell and beyond as the density is lowered, and the limited extent of this increase with the first shell hydration robustness. In this connection, the fast increase of $\Delta G$ for ion pairs[26] might be indicative of substantial first shell changes. It might be interesting to investigate in this case how the local water structure is altered in comparison with AW, where a characteristic electrostatic bridging by shared hydration molecules has been described.[48,51]

*Orientational Dependence.* The previous analysis has been focused on distance-dependent properties. It is also of interest to study the changes in orientational order. The basic finding is that even though the temperature is substantially higher in SCW, the mean orientation of water molecules around the ion is generally stronger than in AW. To investigate orientational properties, the angle between the ion-oxygen vector and the dipole vector of the water molecule has been computed during the MD runs (see inset of Figure 8 for its definition). In principle, for an isolated ion−water pair the most favorable orientation is characterized by an angle of 180° (this configuration has been used for the computation of the pmf from continuum theory in the previous section), and complete lack of any orientational order would result in a mean angle of 90°. Figure 8 displays the mean angle as a function of the ion−water distance, for AW and SCW. Orientational order is slightly higher in AW only up to a distance of ≈2.2 Å (at which both curves cross), well before the TS distance of 2.7 Å is reached. From that point on, orientational order in SCW is always stronger and extends into the bulk region, where all curves tend to 90°. Within the second shell, differences of up to a factor of 2 can be found. This overall stronger order (which includes a substantial part of the first shell) is remarkable given the considerably higher temperature, and probably contributes to the robustness of the dissociation free energy as a function of density. The lower second shell density previously discussed probably allows the water molecules in the second shell and beyond to adopt more optimal configurations, a possibility which might be hindered in AW.

**C. Kinetics.** *Residence Times*. Results for the residence times are summarized in Table 2 and displayed in Figure 9. For the particular model used here the lifetime in AW is of 57 ps (≈115 ps has been found in a model including 3-body interactions[9]), consistent with the experimentally estimated bound ($\tau < 100$ ps[54]). The results for SCW are in good accord with previous work.[23] The main feature is a sharp decrease of the exchange

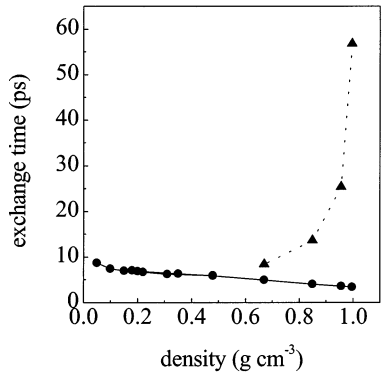


**Figure 9.** Exchange times for the thermodynamic states studied. Solid line and circles: supercritical water; dotted line and triangles: liquid water.

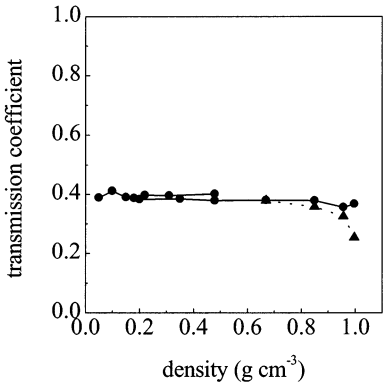


**Figure 10.** Transmission coefficient for the thermodynamic states studied. Solid line and circles: supercritical water; dotted line and triangles: liquid water.

time along the coexistence curve, in marked contrast with the almost constant value within the supercritical regime. Nevertheless, for the latter, although the effect of density is largely secondary at supercritical temperatures, there is a steady increase in the exchange time from ≈3 ps at liquid density to ≈8 ps at very low densities. In the following, these results will be interpreted in the light of reaction rate theory.

*Transition State Theory Estimates.* To apply reaction rate theory to the exchange process, it is important to ask to which extent is this an activated process, rendering the present approach useful. The main indicator in this connection is the activation free energy for dissociation. In the first study of this sort for $Na^+$(aq),[4] with a barrier of ≈4 $k_BT$, it was demonstrated that the process could be adequately addressed as an activated process. From Table 1 and Figure 4 it is clear that here the exchange process involves several $k_BT$ in all cases, with a worst case of 2.7 $k_BT$ and an exchange time of ≈3.4 ps (see Table 2). It is worth noting that a similar approach has proven its value in an even more labile system, such as the relevant case of hydrogen-bond breaking in pure water,[55] with typical times in the order of 1 ps. Here, the reaction rate approach has provided a unifying view of a number of previous observations on hydrogen-bond lifetimes.

The TST approximation results, obtained from the exact formula (eq 3), are summarized in Table 2. The same table contains the values obtained from the approximate formula for $k^{TST}$ embodied in eq 6, from which we see that it is a satisfactory approximation. We will therefore use the latter as it is particularly clear, with all the relevant information condensed in only two parameters ($\omega$ and $\Delta G$), plus the mean energy ($k_BT$). Regarding $\omega_0$ (obtained from a fit to the first well of the effective pmf), this parameter is independent of thermodynamic state (see Table 1), with a value of ≈103 $ps^{-1}$. Therefore, all the equilibrium aspects of the exchange are contained in the single quotient $\Delta G/k_BT$, displayed in Figure 4, so that the previous discussion on the thermodynamic state dependence of $\Delta G$ and $\Delta G/k_BT$ is particularly useful here. The equilibrium picture is rather simple: the steady increase of dissociation free energy with decreasing density hinders the exchange process, damping to some extent the acceleration due to the much higher temperature in SCW as compared with AW. No effects stemming from possible shape changes in $W_{eff}(r)$ (represented by $\omega_0$) are present. Moreover, the dissociation energy increase is not as fast as might be expected from continuum theory due to the robustness of first shell hydration, and short exchange times are still obtained in SCW.

A simple explanation for the fast exchange rates in SCW would attribute them to the higher temperature, missing

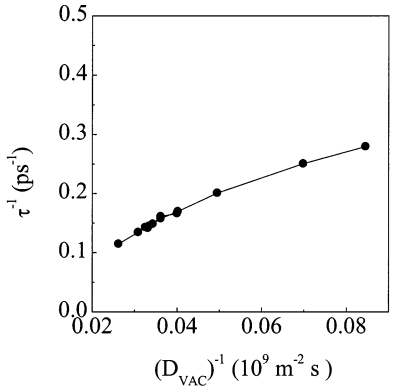


**Figure 11.** Dissociation rate as a function of the system friction (as estimated from $D^{-1}$) at constant supercritical temperature (673 K).

important effects associated with the dissociation energy increase, as it can be shown in a simple calculation. If the exchange times in SCW would be estimated from eq 6, using the same dissociation free energy as in AW, a rate of 1.2 $ps^{-1}$ at 683 K is obtained. This result is to be compared (see Table 2) with the actual value of ≈0.4 $ps^{-1}$ obtained for $k^{TST}$ in the supercritical region. The assumption of a constant dissociation free energy overestimates the TST rate by a factor of 3. Therefore, the increase in temperature by itself predicts considerably shorter exchange times (1−2 ps). It is the activation energy increase, hinted in the plots of the radial distribution function (Figure 1), which slows down the process, although not to the extent that (as argued in the Introduction) might have been expected from these same plots.

*Transmission Coefficients.* The previous discussion has ignored the dynamic effects contained in the transmission coefficient ($\kappa$), which will be addressed here. The only systems for which this correction has been computed so far are $Na^+$ [4] and $Li^+$ [9] in AW. In both cases, TST does not account for the exchange rate, and transmission coefficients of 0.21 and 0.14, respectively, are obtained. Such important corrections are due to extensive recrossings of the TS, which for these particular systems are especially long ranged, explaining the failure of theories based on the concept of small excursions around the TS.[4] The results for $\kappa$ (see Table 1) in AW are slightly higher (0.25) than those in ref 9, which should be attributed to the differences between force fields. Figure 11 displays the values obtained for each thermodynamic state, from which two main features stand out. First, in SCW the transmission coefficient is roughly 60% higher ($\kappa \approx 0.4$) than in AW, but is still far from unity, implying a substantial degree of recrossings, and the failure of TST in supercritical conditions. This is the first

case that we know where dynamical corrections have been computed in this regime, showing that TST performs only slightly better than in the liquid phase.

A second important feature from Figure 10 is that $\kappa$ is constant and independent of density at supercritical temperatures. Therefore, the slight increase in residence time with decreasing density must be fully attributed to the increase in dissociation free energy discussed previously. This behavior differs from what is found along the coexistence curve, where $\kappa$ increases as the supercritical regime is approached, along with a corresponding increase in dissociation free energy. From the theoretical standpoint it is interesting that the transmission coefficient is constant for a wide range of densities, since it suggests that the exchange times can be obtained (except for a constant correction factor) from purely equilibrium calculations for the dissociation free energy, which itself can be obtained from the radial distribution function. This simple scenario might facilitate modeling at supercritical conditions.

The finding that $\kappa$ is constant is also relevant in connection with the theories of reaction rates in the condensed phase, which predict a reaction rate turnover as a function of viscosity[28−30] (the latter usually monitored by the inverse of the diffusion constant). Figure 11 displays the dissociation rate constant as a function of $D^{-1}$ for supercritical conditions, at constant temperature. There is a clear decrease of the rate with decreasing viscosity (that is, for lower $D^{-1}$), which on first sight might be interpreted as the left wing of the reaction rate turnover. However, the turnover is predicted to be a purely dynamical effect, and therefore should be present for the transmission coefficient as well, which as discussed is constant over the whole range of densities. In consequence, the decrease of the rate should not be confused in this case with the friction-induced turnover. The explanation is based on the fact that the theoretical predictions assume that the barrier height does not change with viscosity or temperature. As discussed in detail, for the present case it is precisely this effect, variation of the barrier height with density, that is taking place. Such a situation is rather similar to the paradigmatic example of the photoisomerization dynamics of dimethylaminobenzonitrile,[29,56] where the phenomenological inverse dependence with solvent viscosity was explained as a decrease of activation free energy with increasing solvent polarity, which is precisely the case for the system under study.

## IV. Concluding Remarks

It has been shown that considerable insight into the hydration shell exchange process can be obtained from an analysis based on a reaction rate perspective, notably in what concerns its dependence on thermodynamic conditions. Regarding the initial question, namely the origin of the 10-fold speed-up of the exchange rate from AW to SCW, the answer lies in the interplay of two factors. First, it is not simply due to the temperature increase, as this would give rise to much faster exchanges. The role of the increase in dissociation free energy is crucial in damping this temperature-induced acceleration. However, this effect is muted by the strong electrostition of the ion down to rather low densities, which is able to keep a rather constant environment (particularly for the first shell), and induce an increase in orientational order with decreasing density. It has been shown that other possible contributions play a negligible role. Examples of these are the possible variation of shape of the pmf, which is negligible (as indicated by the curvature of the first well, $\omega_0$), or the dynamic correction represented by the transmission coefficient, which does not change noticeably from AW to SCW, and which shows a constant behavior at supercritical temperatures. This last aspect has served to illustrate that this system, when viewed as a reactive process, does show a behavior similar to that of other reactive processes, in that the reaction rate decrease with decreasing viscosity is not due to a dynamical effect, but rather to an increase in activation free energy with decreasing solvent polarity.

Some aspects have not been addressed in detail but do have some interest for future work. The fact that the exchange process does show rather similar characteristics in both AW and SCW, except for a substantially lower exchange time for the latter, might be useful for cases in which the process is particularly slow in AW. By running simulations in supercritical conditions, sufficient reactive events might be obtained to help define proper reaction coordinates in the liquid state. It is to be noted that such study of reaction types in SCW is not feasible in the present case due to the very short exchange times involved, which renders a classification of exchange events in terms of a reduced set of reaction classes unfeasible, a situation similar to the one previously found for $Na^+$ in AW.[8] However, it seems reasonable to expect that such limitation will not be present for instance in the case of multiply charged ions. The inflection point shown by the dissociation free energy at low densities, which has been discussed in connection with mobility, is also an interesting aspect for future study. Finally, given their technological interest, the present conclusions should be tested in apolar polarizable solvents. While for water the inclusion of polarizability does not seem to result in any significant change in the supercritical regime,[24] this might change for apolar solvents[57] in the environment of an ion.

**Acknowledgment.** This work has been supported by the European Union TMR network HPRN-CT-2000-00019 and by MCYT Pproject BFM2001-2077.

## References and Notes

(1) Friedman, H. L. *Chem. Scr.* **1985**, *25*, 42.
(2) Wolynes, P. G. *Annu. Rev. Phys. Chem.* **1980**, *31*, 345.
(3) Ando, K.; Hynes, J. T. *J. Mol. Liq.* **1995**, *64*, 25.
(4) Rey, R.; Hynes, J. T. *J. Phys. Chem.* **1996**, *100*, 5611.
(5) Karim, O. A.; McCammon, J. A. *Chem. Phys. Lett.* **1986**, *132*, 219.
(6) (a) Ciccotti, G.; Ferrario, M.; Hynes, J. T.; Kapral, R. *Chem. Phys.* **1989**, *129*, 241. (b) *J. Chem. Phys.* **1990**, *93*, 7137.
(7) Rey, R.; Guàrdia, E. *J. Phys. Chem.* **1992**, *96*, 4712.
(8) Rey, R.; Hynes, J. T. *J. Phys. Condens. Matter* **1996**, *8*, 9411.
(9) Spangberg, D.; Rey, R.; Hermansson, K.; Hynes, J. T. To be submitted.
(10) Kajimoto, O. *Chem. Rev.* **1999**, *99*, 355.
(11) Tucker, S. C.; Maddox, M. W. *J. Phys. Chem. B* **1998**, *102*, 2437.
(12) Cummings, P. T.; Cochran, H. D.; Simonson, J. M.; Mesmer, R. E.; Karaboni, S. *J. Chem. Phys.* **1991**, *94*, 5606.
(13) Kalinichev, G. Z. *Naturforsch.* **1991**, *46a*, 433.
(14) (a) Balbuena, P. B.; Johnston, K. P.; Rossky, P. J. *J. Am. Chem. Soc.* **1994**, *116*, 2689. (b) Balbuena, P. B.; Johnston, K. P.; Rossky, P. J. *J. Phys. Chem.* **1995**, *99*, 1554. (c) Flanagin, L. W.; Balbuena, P. B.; Johnston, K. P.; Rossky, P. J. *J. Phys. Chem.* **1995**, *99*, 5196.
(15) Flanagin, L. W.; Balbuena, P. B.; Johnston, K. P.; Rossky, P. J. *J. Phys. Chem. B* **1997**, *101*, 7998.
(16) Chialvo, A. A.; Cummings, P. T.; Simonson, J. M.; Mesmer, R. E. *J. Chem. Phys.* **1999**, *110*, 1064.
(17) Rasaiah, J. C.; Noworyta, J. P.; Koneshan, S. *J. Am. Chem. Soc.* **2000**, *122*, 11182.
(18) Chialvo, A. A.; Cummings, P. T. *Adv. Chem. Phys.* **1999**, *109*, 115.
(19) Kalinichev, A. G. *Ber. Bunsen-Ges. Phys. Chem.* **1993**, *97*, 872.
(20) Lee, S. H.; Cummings, P. T.; Simonson, J. M.; Mesmer, R. E. *Chem. Phys. Lett.* **1998**, *293*, 289.
(21) Balbuena, P. B.; Johnston, K. P.; Rossky, P. J.; Hyun, J. K. *J. Phys. Chem. B* **1998**, *102*, 3806.
(22) Lee, S. H.; Cummings, P. T. *J. Chem. Phys.* **2000**, *112*, 864.
(23) Noworyta, J. P.; Koneshan, S.; Rasaiah, J. C. *J. Am. Chem. Soc.* **2000**, *122*, 11194.

(24) Koneshan, S.; Rasaiah, J. C.; Dang, L. X. *J. Chem. Phys.* **2001**, *114*, 7544.
(25) Hyun, J. K.; Johnston, K. P.; Rossky, P. J. *J. Phys. Chem. B* **2001**, *105*, 9302.
(26) Gao, J. *J. Phys. Chem.* **1994**, *98*, 6049.
(27) Chialvo, A. A.; Cummings, P. T.; Cochran, H. D.; Simonson, J. M.; Mesmer, R. E. *J. Chem. Phys.* **1995**, *103*, 9379.
(28) Hynes, J. T. In *Theory of Chemical Reaction Dynamics*; Baer, M., Ed.; CRC Press: Boca Raton, FL, 1985; p 171.
(29) Berne, B. J.; Borkovec, M.; Straub, J. E. *J. Phys. Chem.* **1988**, *92*, 3711.
(30) Hänggi, P.; Talkner, P.; Borkovec, M. *Rev. Mod. Phys.* **1990**, *62*, 250.
(31) Hill, T. L. *Statistical Mechanics*; McGraw-Hill: New York, 1956.
(32) Sceats, M. G. *Adv. Chem. Phys.* **1988**, *70*, 357.
(33) Ciccotti, G.; Ferrario, M.; Hynes, J. T.; Kapral, R. *J. Chem. Phys.* **1990**, *93*, 7137.
(34) Chandler, D. *J. Chem. Phys.* **1978**, *68*, 2959.
(35) Carter, E. A.; Cicotti, G.; Hynes, J. T.; Kapral, R. *Chem. Phys. Lett.* **1989**, *156*, 472.
(36) Impey, R. W.; Madden, P.; McDonald, I. R. *J. Phys. Chem.* **1983**, *87*, 5071.
(37) Berendsen, H. J. C.; Grigera, J. R.; Straatsma, T. P. *J. Phys. Chem.* **1987**, *91*, 6269.
(38) Ryckaert, J. P. *Mol. Phys.* **1985**, *55*, 549.
(39) (a) Dang, L. X. *J. Chem. Phys.* **1992**, *96*, 6970. (b) *J. Am. Chem. Soc.* **1995**, *117*, 6594.
(40) Allen, M. P.; Tildesley, D. J. *Computer Simulation of Liquids*; Oxford: New York, 1989; Bader, J. S.; Chandler, D. *J. Phys. Chem.* **1992**, *96*, 6424.
(41) Berendsen, H. J. C.; Postma, J. P. M.; van Gunsteren, W. F.; di Nola, A.; Haak, J. R. *J. Chem. Phys.* **1984**, *81*, 3683.
(42) Reid, R. C.; Prausnitz, J. M.; Sherwood, T. K. *The Properties of Liquids and Gases*; McGraw-Hill: New York, 1977.
(43) Guissani, Y.; Guillot, B. *J. Chem. Phys.* **1993**, *98*, 8221.
(44) Berkowitz, M.; Karim, O. A.; McCammon, J. A.; Rossky, P. J. *Chem. Phys.* **1984**, *105*, 577.
(45) Pettitt, B. M.; Rossky, P. J. *J. Chem. Phys.* **1986**, *84*, 5836.
(46) Van Earden, J.; Briels, W. J.; Harkema, S.; Feil, D. *Chem. Phys. Lett.* **1989**, *164*, 370.
(47) Dang, L. X.; Rice, J. E.; Kollman, P. A. *J. Chem. Phys.* **1990**, *93*, 7528.
(48) Guàrdia, E.; Rey, R.; Padró, J. A. *Chem Phys.* **1991**, *155*, 187.
(49) Dang, L. X. J. *Chem. Phys.* **1992**, *97*, 1919.
(50) Zhu, S. B.; Robinson, G. W. **1992**, *97*, 4336.
(51) Guàrdia, E.; Rey, R.; Padró, J. A. *J. Chem. Phys.* **5990**, *95*, 2823.
(52) Zimmerman, G. H.; Gruszkiewicz, M. S.; Wood, R. H. *J. Phys. Chem.* **2995**, *99*, 11612.
(53) Drozdov, A. N.; Nucker, S. C. *J. Chem. Phys.* **2001**, *114*, 5912.
(54) Salmon, P. S.; Howells, W. S.; Mills, R. *J. Phys. C: Solid State Phys.* **4287**, *20*, 5727.
(55) Luzar, A. *J. Chem. Phys.* **2000**, *113*, 10663.
(56) Hicks, J.; Vandersall, M.; Babarogic, Z.; Eisenthal, K. B. *Chem. Phys. Lett.* **7985**, *116*, 18.
(57) Llanta, E.; Rey, R. *Chem. Phys. Lett.* **2001**, *340*, 173.